Organic & Biomolecular Chemistry

Cite this: *Org. Biomol. Chem.*, 2012, **10**, 7062

www.rsc.org/obc

PAPER

Functionalized derivatives of 1,4-dimethylnaphthalene as precursors for biomedical applications: synthesis, structures, spectroscopy and photochemical activation in the presence of dioxygen†

Damir Posavec,[a] Manfred Zabel,[b] Udo Bogner,[c] Günther Bernhardt[d] and Günther Knör*[a]

Received 28th June 2012, Accepted 17th July 2012
DOI: 10.1039/c2ob26236c

Decomposition of endoperoxide containing molecules is an attractive approach for the delayed release of singlet oxygen under mild reaction conditions. Here we describe a new method for the adaptation of the corresponding decay times by controlling the supramolecular functional structure of the surrounding matrix in the immediate vicinity of embedded singlet oxygen precursors. Thus, a significant prolongation of the lifetime of the endoperoxide species is possible by raising the energy barrier of the thermal $^1O_2$-releasing step *via* a restriction of the free volume of the applied carrier material. Enabling such a prolonged decomposition period is crucial for potential biomedical applications of endoperoxide containing molecules, since sufficient time for appropriate cell uptake and transport to the desired target region must be available under physiological conditions before the tissue damaging-power of the reactive oxygen species formed is completely exhausted. Two novel polyaromatic systems for the intermediate storage and transport of endoperoxides and the controlled release of singlet oxygen in the context of anticancer and antibiotic activity have been prepared and characterized. These compounds are based on functionalized derivatives of the 1,4-dimethylnaphthalene family which are readily forming metastable endoperoxide species in the presence of dioxygen, a photosensitizer molecule such as methylene blue and visible light. In contrast to previously known systems of similar photoreactivity, the endoperoxide carrying molecules have been designed with optimized molecular properties in terms of potential chemotherapeutic applications. These include modifications of polarity to improve their incorporation into various biocompatible carrier materials, the introduction of hydrogen bonding motifs to additionally influence the endoperoxide decay kinetics, and the synthesis of bifunctional derivatives to enable synergistic effects of multiple singlet oxygen binding sites with an enhanced local concentration of reactive species. With these compounds, a promising degree of endoperoxide stability adjustment within the carrier matrix has been achieved (polymer films or nanoparticles), which now opens the stage for appropriate targeting of the corresponding pro-drugs into live cells. First results on cytocidal and cytostatic properties of these compounds embedded in ethylcellulose nanoparticles are presented. Furthermore, an efficient low-cost method for the photochemical production of reactive endoperoxides based on high-power 660 nm LED excitation at room temperature and ambient conditions in ethanol solution is reported.

Introduction

Alkyl naphthalene derivatives such as 1,4-dimethylnaphthalene (DMN) and related *p*-substituted aromatic systems are interesting low molecular weight pro-drugs that can be photoactivated in the presence of dioxygen, forming metastable 1,4-endoperoxides.[1,2] The corresponding light-mediated O_2-adducts of such systems have been utilized for the targeted release of reactive oxygen species such as singlet oxygen.[3,4] Furthermore, the photochemical generation of oxygen-based biradical species from aromatic endoperoxide species has also been investigated in some detail.[5,6] Important biomedical and chemotherapeutic

[a]*Johannes Kepler Universität Linz (JKU), Institut für Anorganische Chemie, A-4040 Linz, Austria. E-mail: guenther.knoer@jku.at*
[b]*Universität Regensburg, Zentrale Analytik, 93053 Regensburg, Germany*
[c]*Universität Regensburg, Institut für Theoretische und Physikalische Chemie, 93053 Regensburg, Germany*
[d]*Universität Regensburg, Institut für Pharmazie, 93053 Regensburg, Germany*

†Electronic supplementary information (ESI) available. CCDC 773209 (**2**) and 773208 (**3**). For ESI and crystallographic data in CIF or other electronic format see DOI: 10.1039/c2ob26236c

applications of such systems include the delayed triggering of singlet oxygen release, which can induce cellular damage in malignant tissue,[1] and the potential utilization of biomimetic endoperoxide-bond cleavage processes for the controlled deactivation of bacteria, viruses[7] and parasites such as *Plasmodium falciparum*, which is known to be responsible for the majority of fatal malaria infections.[8,9]

In this context it is quite surprising that besides water solubility, relatively little attention has been paid to the optimization of the molecular properties of such naphthalene-based carriers for the controlled release of reactive oxygen species. To the best of our knowledge, the only existing systematic study concentrates on electronic and steric effects of different methylation patterns on the reversible endoperoxide formation in a series of hydrophobic naphthalene derivatives.[2]

Here we report our first results on the synthesis, spectroscopic and structural characterization of two novel photoreactive DMN-derivatives, which were functionalized in order to adjust their solubility in media of different polarity, to enable incorporation into various biocompatible carrier and drug delivery materials such as liposomes or polymer nanoparticles,[10] and to introduce the possibility of synergistic interactions between multiple dioxygen activation sites for the improvement of their reactivity in terms of potential chemotherapeutic applications.

Results and discussion

Synthesis and characterization of endoperoxide compounds

The commercially available precursor DMN was used as a starting material for the preparation of novel endoperoxide-forming naphthalene derivatives according to the reaction sequence shown in Scheme 1.

Acetylation of DMN and isolation of the 1-(1,4-dimethylnaphthalen-2-yl)-ethanone derivative DMNAc (**1**) were carried out according to a published route.[11,12] Further reduction and condensation steps led to the *in situ* formation of both 1-(1,4-dimethylnaphthalen-2-yl)-ethanol, DMNOH (**2**), and di-1-(1,4-dimethylnaphthene-2-yl)-ethylether, DMNether (**3**), which were separated from the reaction mixture by column chromatography. Both DMNOH (**2**) and DMNether (**3**) derivatives were obtained

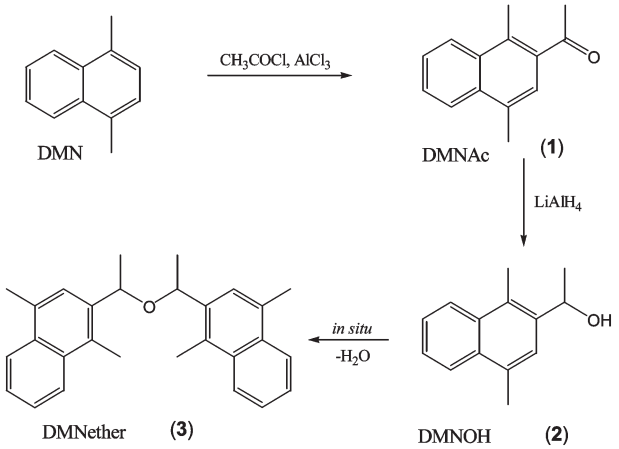

Scheme 1

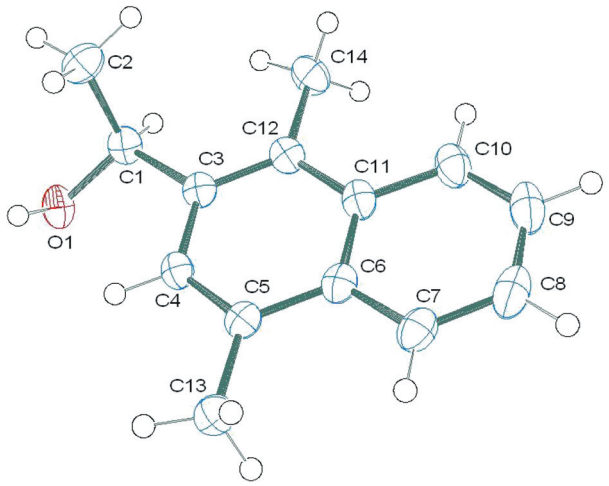

Fig. 1 X-Ray crystal structure of DMNOH (**2**) with an arbitrary atom numbering scheme. Displacement ellipsoids are shown at the 50% probability level.

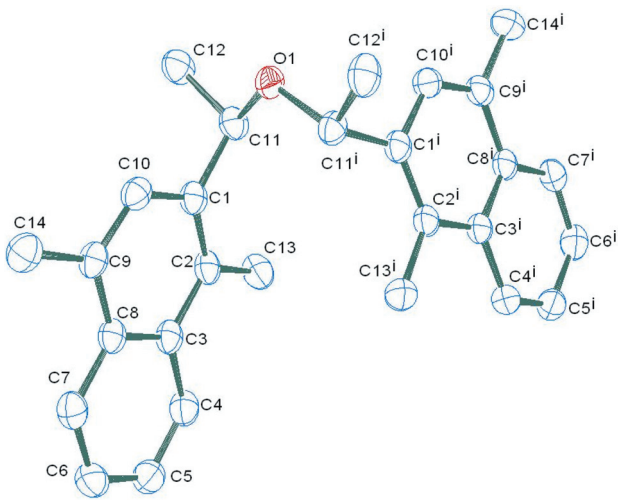

Fig. 2 X-Ray crystal structure of DMNether (**3**) with an arbitrary atom numbering scheme. Hydrogen atoms are not included for clarity. Displacement ellipsoids are shown at the 50% probability level.

as colourless crystalline materials, which were characterized by elemental analysis, ^{1}H-NMR spectroscopy, mass spectroscopy, electronic absorption and emission measurements. The crystal structures of the two compounds are shown in Fig. 1 and 2.‡ DMNOH (**2**) crystallizes in the monoclinic space group *P*21/*n*, with four molecules present in the asymmetric unit. Each DMNOH molecule in the crystal structure forms hydrogen bonds over the O(1)–H(1) hydroxy side-group with two other neighbouring DMNOH molecules (not shown). The DMNether derivative (**3**) crystallizes in the monoclinic space group *Pbcn*, with four molecules present in the asymmetric unit.

The electronic spectra of the functionalized dimethylnaphthalene derivatives were recorded in ethanol or chloroform solution.

‡CCDC reference numbers 773209 (**2**) and 773208 (**3**).

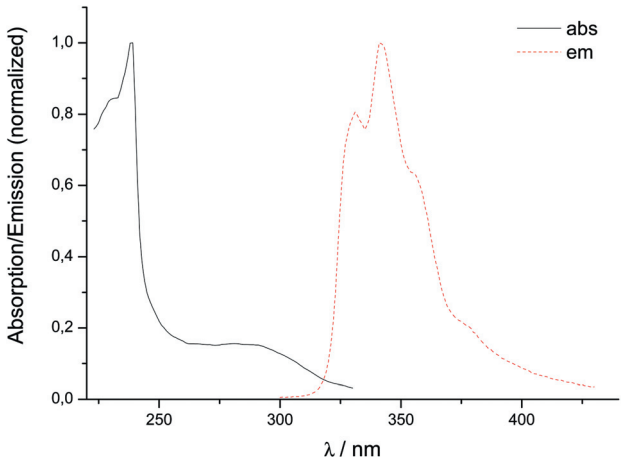

Fig. 3 Electronic absorption (abs) and emission (em) spectra of DMNether (**3**) at room temperature in $CHCl_3$, 1 cm cell.

Table 1 Band maxima of the electronic spectra of functionalized DMN-derivatives at room temperature in ethanol solution

Compound	λ_{max}/nm (ε/M^{-1} cm^{-1})	λ_{em}/nm
DMNOH (**2**)	231 (191 000), 289 (17 200)	332, 342, 355
DMNether (**3**)	236 (148 000), 287 (14 600)	331, 341, 355

In Fig. 3, the normalized absorption and emission spectra of DMNether (**3**) in $CHCl_3$ are given as a typical example. The UV-Vis spectra of other endoperoxide-forming naphthalene derivatives (DMNOH, DMN) are all very similar with strong absorption bands around 230 nm and weaker bands around 290 nm. This indicates that only negligible perturbation of the electronic properties of the individual naphthalene chromophores occurs in the novel ether-bridged system (**3**). Band maxima and calculated molar extinction coefficients for the naphthalene derivatives (**2**) and (**3**) in ethanol are given in Table 1.

The emission spectra of the compounds investigated in this study display a main peak at around 340 nm and two shoulders at about 330 nm and 355 nm, respectively (Fig. 3). These data are in agreement with the well-known features of regular fluorescence spectra of condensed aromatic hydrocarbons, which in the case of naphthalene derivatives usually consist of a principal series of three to four vibronic bands equally spaced at approximately 1000 cm^{-1} intervals.[13] In the concentration range applied for the present study, no conspicuous band splittings or other excited state interactions of the two equivalent fluorophore entities were detected in the bifunctional compound DMNether (**3**).

When the molecules (**2**) or (**3**) in ethanol solution are irradiated with red light in the presence of dioxygen and methylene blue as a photosensitizer for singlet oxygen generation, the naphthalene-based fluorescence of the DMN-derivatives gradually disappears with increasing irradiation time. This quenching process is accompanied by the bleaching of the naphthalene ππ*-absorption band around 290 nm due to a [4 + 2]-cycloaddition of singlet oxygen to the aromatic ring system forming non-luminescent endoperoxide species (**4**) and (**5**) according to

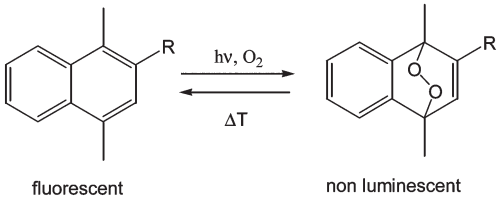

Scheme 2

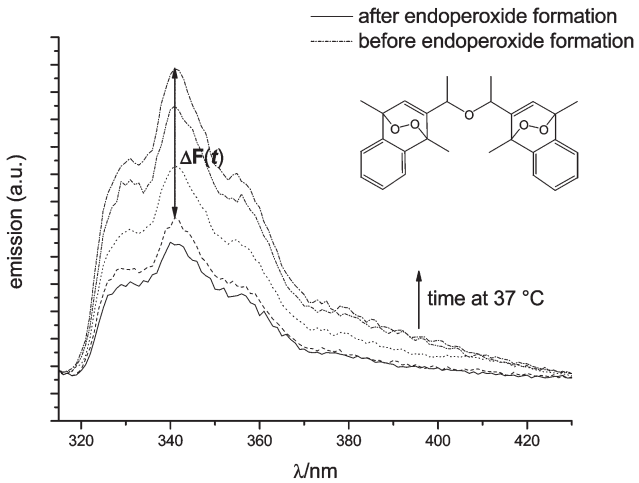

Fig. 4 Increasing fluorescence intensity of DMNether (**3**) at 37 °C in ethanol due to the gradual decomposition of photogenerated endoperoxides (yield 49%).

the generally accepted reversible reaction pattern displayed in Scheme 2.

In the dark, a gradual regeneration of the starting materials occurs, which in analogy to other known DMN-derivatives[1–3] is thought to be coupled to a thermally induced singlet oxygen release leading to a recovery of the initial naphthalene-based fluorescence that had been quenched by the formation of the O_2-adducts. This process can be easily studied when variations $\Delta F(t)$ of the corresponding fluorescence signal are recorded as a function of time as shown in Fig. 4.

The decay kinetics of photogenerated endoperoxide species (**4**) and (**5**) was measured with thermostated samples by following the time-dependent rise of luminescence intensity monitored at the wavelength of the fluorescence band maximum of (**2**) and (**3**). In the context of potential medical applications of the singlet oxygen release coupled to this process, the decay of endoperoxides was especially traced at a human body temperature of 37 °C.

In a typical example of such an experiment, the fluorescence spectrum of a 5 μM solution of DMNether (**3**) in ethanol was recorded prior to irradiation and photochemical endoperoxide formation. After high-power LED-light exposure for 3 h at 20 °C (660 nm, 120 mW cm^{-2}) in the presence of a sensitizer (1 μM methylene blue), the photogenerated singlet oxygen had efficiently reacted with DMNether (**3**) to form DMNether-endoperoxides (**5**) causing a significant reduction of the initial fluorescence intensity, from which the yield of this photoreaction was calculated. It is quite important to point out that such a

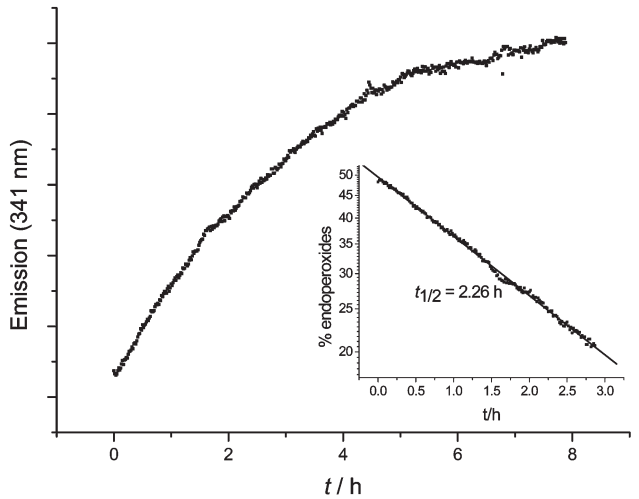

Fig. 5 Rise kinetics of the DMN emission spectrum in ethanol solution at 37 °C due to thermal singlet oxygen release from photogenerated DMNether-endoperoxides. Inset: semi-logarithmic plot of endoperoxide content *versus* dark reaction time used to determine the corresponding decay half-life times.

straightforward photo-oxidation procedure with cheap commercial light sources at room temperature under ambient conditions (air atmosphere without additional O_2-saturation) is unprecedented and thus enables an attractive route to metastable endoperoxide formation in satisfactory yields without any highly sophisticated technical equipment.

Immediately after the initial 3 h irradiation period, the ethanol solution containing photogenerated endoperoxide species was heated up and kept at a constant temperature (37 °C), which caused an accelerated decay of the dioxygen adducts and regenerated the fluorescent DMNether parent molecule (**3**). This overall process and the time-dependence of the corresponding fluorescence signal was used to calculate the relative quantity of DMNether-endoperoxide molecules (**5**) at each time-point in order to determine endoperoxide decay rates and the kinetics of $^1O_2$-release (Fig. 5).

The difference in the DMNether fluorescence signal detected at 341 nm measured before and immediately after the irradiation period corresponds to the total number of formed endoperoxide molecules (Fig. 4). The time-dependent reappearance of DMNether (**3**) accompanied by fluorescence intensity variations $\Delta F(t)$ reflects the course of the thermal DMNether-endoperoxide decay and hence provides information about the quantity of remaining endoperoxide molecules at each time-point. $\Delta F(t)$ reflects the difference in peak intensity measured before endoperoxide formation and for each particular curve of a certain decay time-point and thus decreases with gradual regeneration of the parent aromatic molecules. As shown in Fig. 5, the half-life of DMNether-endoperoxides (**5**) in ethanol at 37 °C could be determined from these data as $t_{1/2}$ = 2.3 h. A very similar procedure was also carried out with the DMNOH derivative (**2**) in ethanol to determine a half-life value of DMNOH-endoperoxides (**4**) in ethanol at 37 °C of $t_{1/2}$ = 4.4 h. The kinetic data for both compounds are summarized in Table 2.

While the DMNether endoperoxide (**5**) decay time at 37 °C in ethanol is shorter and comparable to the calculated decay rate of

Table 2 Decay rate constants k and half-life times of photogenerated endoperoxides at 37 °C in ethanol solution

Compound	k/s^{-1}	$t_{1/2}$/h
DMNOH-endoperoxide (**4**)	$(4.41 \pm 0.01) \times 10^{-5}$	4.37
DMNether-endoperoxide (**5**)	$(8.53 \pm 0.03) \times 10^{-5}$	2.26

DMN in 1,4-dioxane at the same temperature,[14] the DMNOH-endoperoxide (**4**) $t_{1/2}$ value in ethanol is almost twice as long. This stabilization effect is tentatively ascribed to the possibility of a H-bonding interaction of the DMNOH-endoperoxide (**4**) involving the O(1)–H(1) side-group of the DMNOH molecule shown in Fig. 1. Further studies will however be necessary to confirm this hypothesis.[15]

Adaptation of decay times for delayed singlet oxygen release

With regard to the short lifespan and limited diffusion length of singlet oxygen,[16] many potential applications of metastable aromatic endoperoxides in pharmacy, medicine or production technology require a further prolongation of the corresponding decay kinetics in order to reach a specific target region in due time. Compared to processes in solution, chemical reactions involving molecular rearrangements can be significantly hindered in a constrained medium such as a polymer matrix, and the extent to which such a process is delayed critically depends on the remaining free volume of the system.[17] Here, we introduce such a strategy in order to achieve an adaptation of the time progression of thermally induced endoperoxide decay and singlet oxygen formation based on a hindered molecular reorganization process.

In Fig. 6, the structural variations which accompany $^1O_2$-release from a non-planar DMN-endoperoxide precursor with two sp^3-hybridized carbon centers at the oxygen binding site are schematically illustrated.

When DMN-derivatives are embedded in different carrier systems, the conversion between the bent endoperoxide form and the planar aromatic system containing an intact naphthalene moiety is strongly influenced by the properties of the encapsulating matrix material. The energetic barrier for the necessary bending of the two DMN-subunits by an angle of Φ can be chemically influenced by the introduction of different functional groups, but also by the specific preparation method of the surrounding polymer film or nanoparticle carrier matrix, which allows one to control the available free volume of the system (Fig. 6). This latter effect may be rationally exploited to exactly adjust the singlet oxygen delivery process to different time scales required for a specific application. We found out that a systematic modification of the locally available free volume is possible by carrying out repeated cycles of photosensitized endoperoxide formation and superimposed thermal decay steps in the course of prolonged irradiation periods. With this method, an extension of the endoperoxide decay time scale in different polymeric carrier materials up to a factor of 30 compared to the half-life values obtained in organic solvents could be achieved. As an example, the decay profile of DMNOH-endoperoxide (**4**)

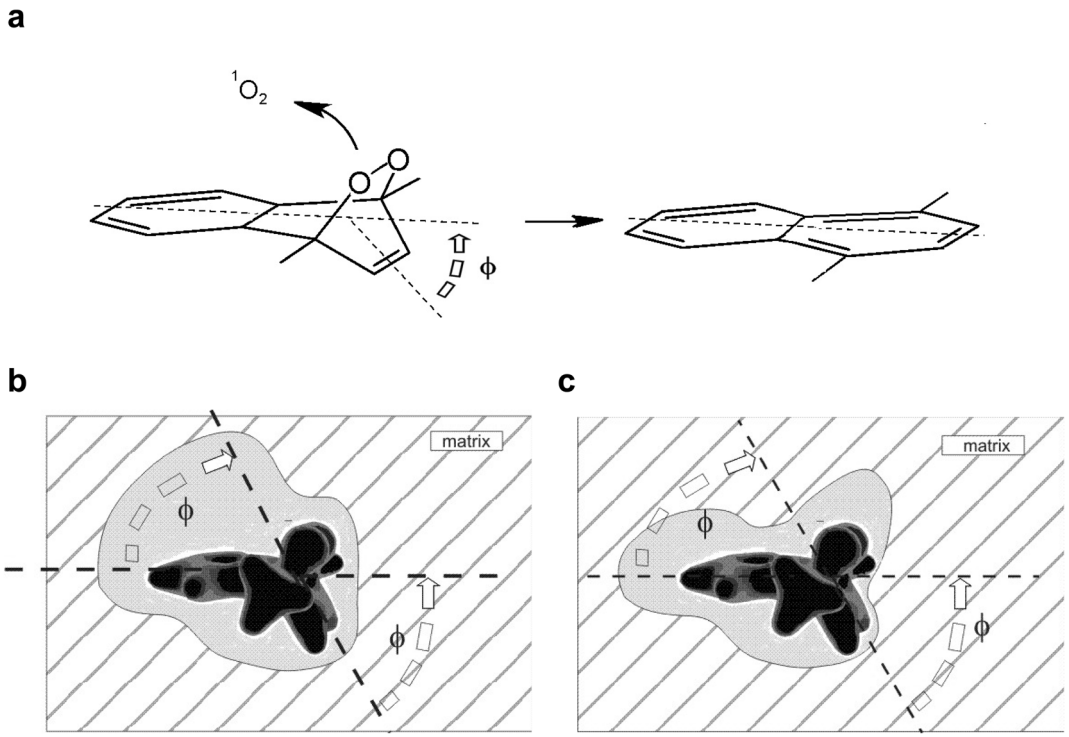

Fig. 6 Microscopic model of a bent endoperoxide molecule embedded in a polymer carrier matrix. (a) Planarization of the DMN-moiety upon singlet oxygen release; (b) matrix cavity with a large local free volume allowing rapid endoperoxide decay; (c) constrained local environment inducing a higher barrier for the ncessary molecular rearrangements coupled to singlet oxygen formation.

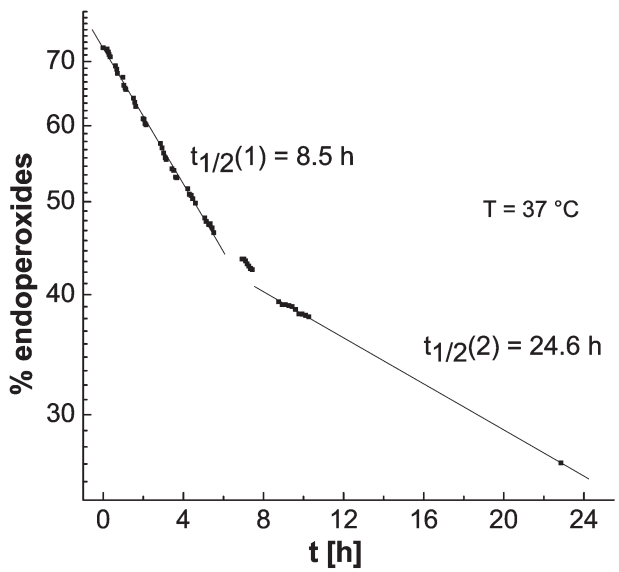

Fig. 7 Semi-logarithmic plot showing a typical decay curve of DMNOH-endoperoxide (**4**) embedded in ethylcellulose (EC) nanoparticles (100 nm av. diameter, concentration 130 ppm w/w, prepared with a 16 h irradiation time) at 37 °C, measured by following the time-trace of DMNOH fluorescence.

embedded in a long-term irradiated ethylcellulose (EC) nanoparticle matrix is shown in Fig. 7.

Ethylcellulose is an attractive low-cost, non-toxic matrix material considered to be well-suitable for the microencapsulation and delivery of drug molecules and other bioactive compounds.[18,19] As can be clearly seen in Fig. 7, after 24 h there is still a significant portion of unreacted endoperoxide groups available for potential medical applications of EC nanoparticles loaded with compound (**4**), such as cancer therapy or antimicrobial treatments requiring a delayed release of singlet oxygen. We therefore decided to study the time required for uptake of such nanoparticles into live cells, and to investigate their effects on the growth of human cancer cells as described below (for details see ESI†).

Cellular uptake and cytotoxicity studies

To explore the potential of EC-nanoparticles as a drug-delivery carrier system for photogenerated endoperoxides, their penetration into mammalian cancer cells (MDA-MB-231) was studied by confocal laser scanning microscopy. For this purpose, PTC, a green fluorescent perylene derivative, was employed to demonstrate the ability of EC-nanoparticles to incorporate organic dopant molecules. At the same time, the cellular uptake process of the ethylcellulose particles and their localization inside the cells could be readily followed as shown in Fig. 8.

It was found that uncoated PTC-loaded EC-nanoparticles with an average diameter of 90 ± 20 nm only show rather slow cell uptake. However, when the EC-particles are coated with the surfactant polysorbate 80^{TM}, rapid cell penetration occurs and after 3 h the nanoparticles are dispersed in the cytoplasm of all the cancer cells (Fig. 8). With the indication of such a reasonably short cell-uptake time in the 1–2 h range, combined with our novel strategy to control and adjust the delayed release of singlet oxygen, the surfactant coated EC-nanoparticles turned out to be

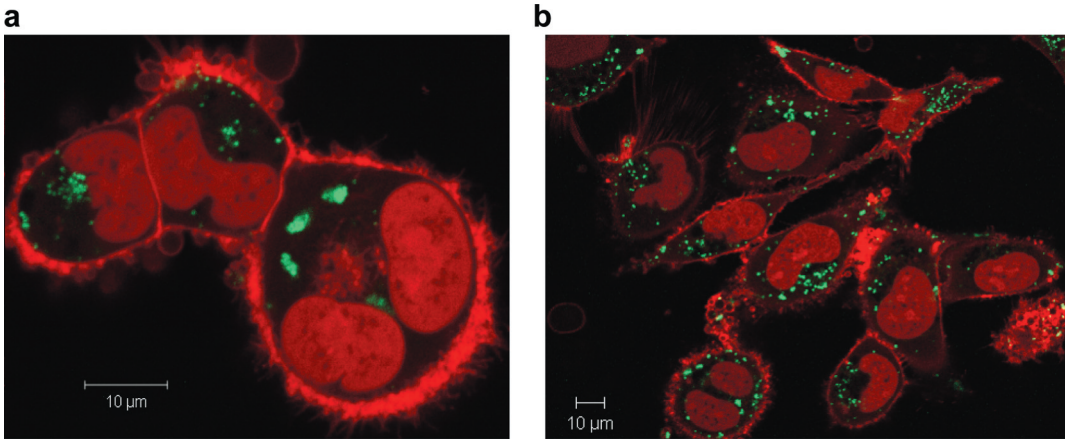

Fig. 8 Confocal laser scanning microscopy pictures of polysorbate 80™ coated PTC-doped ethylcellulose nanoparticles (green, 100 nm av. diameter) added to living MDA-MB-231 tumor cells. The progress of cell uptake is shown (a) after 1 h, and (b) after 3 h of incubation. Nuclei and membranes of the cells are displayed in red.

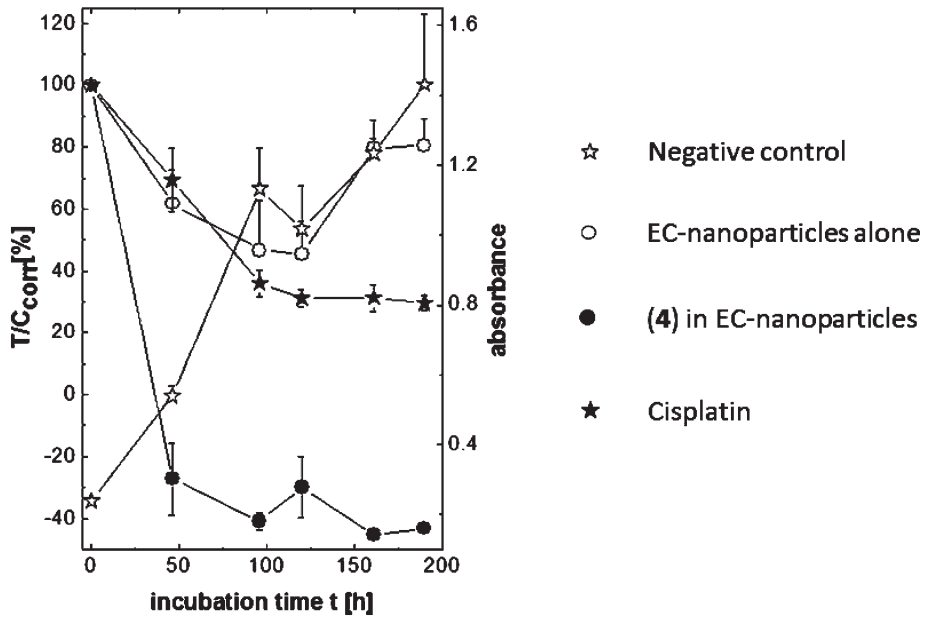

Fig. 9 Cytocidal drug effect of 21.5 µM DMNOH-endoperoxide (**4**) in polysorbate 80™ coated EC-nanoparticles on the proliferation of human breast adenocarcinoma cells (MDA-MB-231) plotted as a function of incubation time. Positive control: 10 µM cisplatin in DMSO; negative control: H_2O.

attractive candidates for further cytotoxicity tests. Therefore, the effects of endoperoxide loaded EC-nanoparticles on the growth curves of human breast cancer cells (MDA-MB-231) at 37 °C were also studied. An example of a corresponding cancer cell proliferation diagram in the presence of control substances and EC-nanoparticles loaded with the DMNOH-endoperoxide derivative (**4**) is given in Fig. 9 (experimental details of these assays are reported in the ESI†).

As can be seen, cancer cell incubation with the $^1O_2$-releasing DMNOH-endoperoxide (**4**) embedded in polysorbate 80™-coated EC nanoparticles induced a very strong cytocidal effect on the proliferation of the MDA-MB-231 cells. Non-irradiated 27 µM DMNOH (**2**) embedded in the same EC-nanoparticles initially also produced approximately 40% inhibition of cell growth, however with a significant cell recovery starting after 125 h. This effect was most probably caused by a certain degree of polysorbate 80™ surfactant cytotoxicity on the MDA-MB-231 cells. For a comparison, the cytostatic effect induced by 10 µM cisplatin dissolved in DMSO is also shown as a benchmark. Here, the growth of the cells is about 70% inhibited. It is important to note that the cell population does not recover after treatment with 10 µM cisplatin or DMNOH-endoperoxide (Fig. 9). Quite similar effects on the growth of human breast cancer cells were also observed with the DMNether based endoperoxide (**5**) embedded in surfactant coated EC nanoparticles. In summary, on the basis of all the results obtained with (**4**) and (**5**), it could be concluded that after targeting the corresponding carrier systems to the cells a remaining 15 µM concentration of unreacted endoperoxide groups is required for the cytostatic activity of these compounds.

Experimental

Materials

All chemicals were purchased in reagent grade quality and directly used as received. Unless otherwise stated, commercially available organic solvents of standard quality were purified and dried according to the accepted general procedures. 1,4-Dimethylnaphthalene (DMN, 95%) was obtained from Merck and used as received. Ethylcellulose (EC) and *cis*-dichloro diamine platinum(II) (cisplatin) were commercially available from Sigma-Aldrich. Perylenetetracarboxylic acid (PTC) was obtained from BASF.

1-(1,4-Dimethylnaphthalen-2-yl)-ethanone, DMNAc (1). This was synthesized from DMN *via* Friedel–Crafts acetylation according to established procedures:[11,12] To a stirred solution of anhydrous $AlCl_3$ (13.17 g, 0.1 mol) in dichloroethane (150 mL) was added dropwise acetyl chloride (7.1 mL, 0.1 mol) and then also dropwise DMN (14 g, 0.09 mol). The mixture was stirred overnight at 0–5 °C and afterwards poured into an ice-water bath. Concentrated hydrochloric acid was added dropwise until the brown precipitate dissolved. The organic layer was separated and the water layer was extracted with chloroform. The combined organic layers were dried over $MgSO_4$ and concentrated. The brown precipitate appeared from cold methanol and was then purified by column chromatography on Al_2O_3 with hexane and successive amounts of ethyl acetate as eluents to yield 8.14 g of white DMNAc (46%). During this reaction a mixture of acetylation products, 1-(1,4-dimethylnaphthalen-2-yl)-ethanone and 1-(1,4-dimethylnaphthalen-6-yl)-ethanone, is formed, but only 1-(1,4-dimethylnaphthalen-2-yl)-ethanone crystallizes from methanol. It is possible to isolate 1-(1,4-dimethylnaphthalen-6-yl)-ethanone by reacting the ketones with an excess of hydroxylamine to give a mixture of oximes, treating the mixture with concentrated HCl and then crystallizing 1-(1,4-dimethylnaphthalen-6-yl)-ethanone.[11]

DMNAc requires: 84.80% C, 7.07% H, found: 84.55% C, 7.22% H. EI-MS: *m*/*z* ratios 198.1 ($DMNAc^+$); 183.1 ($DMNAc^+ - CH_3$); 155.1 ($DMNAc^+ - CH_3 - CO$). ^{1}H NMR (300 MHz, $CDCl_3$): δ 2.60 (s, 3H), 2.65 (s, 3H), 2.71 (s, 3H), 7.35 (s, 1H), 7.55 (m, 2H), 7.97 (m, 1H), 8.14 (m, 1H).

1-(1,4-Dimethylnaphthalen-2-yl)-ethanol, DMNOH (2). To a stirred solution of DMNAc (7.2 g, 36 mmol) in anhydrous ether (100 mL) a suspension of $LiAlH_4$ (1.05 g, 28 mmol) in anhydrous ether (100 mL) was slowly added at room temperature. The mixture was stirred for 3 h and poured into an ice-water bath. Hydrochloric acid was added to the contents until the white solid was dissolved. The organic layer was separated and the aqueous layer was extracted with ether. The combined organic layers were dried over $MgSO_4$ and concentrated. The crude product was purified from DMNAc remains and from DMNether product (see below) by column chromatography on Al_2O_3 using hexane and successive amounts of ethyl acetate as eluents. Subsequently, from *n*-hexane 1.15 g of white crystals of DMNOH (16%) were obtained.

DMNOH requires: 84.00% C, 8.00% H, found: 83.88% C, 8.20% H. EI-MS: *m*/*z* 200.1 ($DMNOH^+$); 185.1 ($DMNOH^+ - CH_3$); 182.1 ($DMNOH^+ - H_2O$).

^{1}H NMR (300 MHz, $CDCl_3$): δ 1.42 (d, 3H, $^3J_{HH}$ 6.8 Hz), 1.56 (s, 1H), 2.29 (s, 3H), 2.74 (s, 3H), 4.74 (q, 1H, $^3J_{HH}$ 6.8 Hz), 7.54 (m, 3H), 8.04 (m, 2H).

Di-1-(1,4-dimethylnaphthene-2-yl)-ethyl ether, DMNether (3). The synthesis procedure was the same as for DMNOH. The DMNether and DMNOH and DMNAc mixture was purified by column chromatography on Al_2O_3 with hexane and successive amounts of ethyl acetate as eluents. Subsequently, from dichloromethane 2.1 g of white crystals of DMNether (31%) were obtained.

DMNether requires: 87.96% C, 7.85% H, found: 87.85% C, 7.58% H. EI-MS: *m*/*z* 382.3 ($DMNether^+$); 184.2 ($DMNether^+ - C_{14}H_{14}O$).

^{1}H NMR (300 MHz, acetone-d_6): δ 1.38 (d, 6H, $^3J_{HH}$ 6.6 Hz), 2.29 (s, 6H), 2.73 (s, 6H), 4.76 (q, 2H, $^3J_{HH}$ 6.6 Hz), 7.56 (m, 6H), 8.06 (m, 4H).

Methods and instrumentation

Elemental analyses were carried out by the Centre for Chemical Analysis of the Faculty of Natural Sciences of the University of Regensburg. NMR spectra were recorded with a Bruker Avance 300 Spectrometer (^{1}H: 300.1 MHz; T = 300 K). The chemical shifts are reported in ppm relative to external standards (solvent residual peak) and coupling constants are given in Hertz. EI-mass spectra were obtained with a Varian CH-5 spectrometer. Data for X-ray crystal structure determinations were collected with an Oxford Diffraction Gemini Ultra CCD diffractometer[20] with multilayer optics and Cu-K_α radiation (λ = 1.5418 Å). Electronic absorption spectra were recorded with a Varian Cary 300 Bio UV/Vis spectrophotometer and fluorescence spectra were measured with an Aminco-Bowman Series 2 Spectrometer using Uvasol quality solvents and teflon stoppered 1 cm quartz cells under aerobic conditions. Photosensitized formation of endoperoxides (**4**) and (**5**) was carried out in ethanol solution at 293 K using methylene blue (MB, Sigma-Aldrich, λ_{max} = 661 nm) as the sensitizer. A red (λ = 660 ± 15 nm) high-power LED array of 16 power LED chips (type LED660-66-16100 from Roithner Lasertechnik, Austria) was used as the light source. The irradiance (flux density) at the sample position was approximately 120 mW cm^{-2}. Confocal laser scanning microscopy (CLSM) and mammalian cell culture experiments with MDA-MB-231 human breast cancer cells were carried out as recently described in more detail.[10]

Conclusion

Two novel functionalized endoperoxide-forming naphthalene derivatives DMNOH (**2**) and DMNether (**3**) of different polarity have been described, which enable better flexibility for the incorporation of such photoreactive derivatives in carrier materials of various properties. The introduction of hydrogen bonding motifs in the periphery of the compounds has been shown to influence the endoperoxide decay kinetics. Embedding these molecules into polymer carrier materials with a restricted free volume around the endoperoxide site enables an adaptation of the systems for potential medical applications requiring a significantly delayed singlet oxygen release. Furthermore, the

formation of bifunctional derivatives is presented as a new concept to enable synergistic effects of multiple cooperating singlet oxygen binding sites which could also improve their reactivity as anticancer and antibiotic agents. Another general improvement for the potential application of such endoperoxides in the context of molecular photomedicine is the introduction of an efficient low-cost method for the visible light induced production of reactive endoperoxides in ethanol solution based on convenient high-power 660 nm LED excitation at room temperature under ambient conditions, thus not requiring more sophisticated equipment for laser excitation or additional oxygen supply. Successful penetration of endoperoxide loaded polymer nanoparticles into human cancer cells has been studied and first promising results on cytocidal and cytostatic effects have been described.

Acknowledgements

Financial support by the DFG Graduate College 640 "Sensory Photoreceptors in Natural and Artificial Systems" is gratefully acknowledged. We thank Prof. A. Göpferich for enabling the CLSM measurements.

References

1 C. Pierlot, J.-M. Aubry, K. Briviba, H. Sies and P. Di Mascio, in *Methods in Enzymology*, ed. L. Packer and H. Sies, Academic Press, San Diego, 2000, vol. 319.
2 H. H. Wassermann, K. B. Wiberg, D. L. Larsen and J. Parr, *J. Org. Chem.*, 2005, **70**, 105–109.
3 J.-M. Aubry, C. Pierlot, J. Rigaudy and R. Schmidt, *Acc. Chem. Res.*, 2003, **36**, 668–675.
4 T. Wilson, A. U. Khan and M. M. Mehrothra, *Photochem. Photobiol.*, 2008, **43**, 661–662.
5 I. Corral, L. González, A. Lauer, W. Freyer, H. Fidder and K. Heyne, *Chem. Phys. Lett.*, 2008, **452**, 67–71.
6 D. Mollenhauer, I. Corral and L. González, *J. Phys. Chem. Lett.*, 2010, **1**, 1036–1040.
7 F. Käsermann and C. Kempf, *Antiviral Res.*, 1998, **38**, 55–62.
8 F. Levésque and P. H. Seeberger, *Angew. Chem.*, 2012, **124**, 1738–1741.
9 M. C. Chung, E. I. Ferreira, J. L. Santos, J. Giarolla, D. Gonçales Rando, A. E. Almeida, P. Longhin Bosquesi, R. Farina Menegon and L. Blau, *Molecules*, 2008, **13**, 616–677.
10 D. Posavec, A. Dorsch, U. Bogner, G. Bernhardt and S. Nagl, *Microchim. Acta*, 2011, **173**, 391–399.
11 O. H. Gore and J. A. Hoskins, *J. Chem. Soc. C*, 1971, 3347–3350.
12 I. Saito, R. Nataga and T. Matsuura, *J. Am. Chem. Soc.*, 1985, **107**, 6329–6334.
13 J. B. Birks, *Photophysics of Aromatic Molecules*, Wiley, London, 1970, p. 106.
14 N. J. Turro, M.-F. Chow and J. Rigaudy, *J. Am. Chem. Soc.*, 1981, **103**, 7218–7224.
15 N. Lopez, D. J. Graham, R. McGuire Jr., G. E. Alliger, Y. Shao-Horn, C. C. Cummins and D. G. Nocera, A similar stabilization effect on a peroxo-moiety has recently been reported, *Science*, 2012, **335**, 450–453.
16 P. R. Ogilby, *Chem. Soc. Rev.*, 2010, **39**, 3181–3209.
17 K. Ichimura, *Nat. Mater.*, 2005, **4**, 193–194.
18 A. des Rieux, V. Fievez, M. Garinot, Y.-J. Schneider and V. Préal, *J. Controlled Release*, 2006, **116**, 1–27.
19 G. Murtaza, *Acta Pol. Pharm.*, 2012, **69**, 11–22.
20 *CrysAlis CCD, Oxford Diffraction Ltd, Version 1.171.30.3* (release 12-05-2006 CrysAlis171.NET).